July 2018

Comparison Of Three Transient Models For Slab Heating/Cooling Systems

Anthony Rey
Concordia University, Canada, anthonyrey.simonnot@gmail.com

Rémi Dumoulin
Concordia University, Canada, remi.dumoulin@outlook.com

Andreas Athienitis
Concordia University, Canada, aathieni@encs.concordia.ca

Comparison of Three Transient Models for Heating/Cooling Systems

Anthony REY[1a]*, Remi DUMOULIN[1b], Andreas K. ATHIENITIS[1c]

[1]Centre for Net-Zero Energy Buildings Studies, Department of Building, Civil and Environmental Engineering, Concordia University,
Montreal, Quebec, Canada
[a]+1 514-848-2424 ext. 7078, an_rey@encs.concordia.ca
[b]+1 514-848-2424 ext. 7078, remi.dumoulin@outlook.com
[c]+1 514-848-2424 ext. 8791, aathieni@encs.concordia.ca

* Corresponding Author

ABSTRACT

Radiant floor heating and cooling systems can be beneficial in various applications such as heating or cooling buildings and in infrastructure applications such as de-icing of bridges and roads as well as snow melting. Such systems usually include a significant amount of thermal mass, thus providing energy flexibility in buildings. Models of embedded-tube radiant systems are therefore useful to predict their behavior (rate of heat transfer and outlet heat-transfer fluid temperature), which can be used for the development of predictive control strategies and optimal control algorithms. As a result, a comparison of different models is conducted in this paper. The TRNSYS simulation software provides three different ways of modeling radiant floor systems (Type 56, Type 653, and Type 993), which are compared in this paper with one another in order to assess their accuracy and limitations. Each approach is compared with measurements from an experimental set-up in a controlled environmental chamber. This paper aims at: (i) evaluating the appropriate model resolution for embedded-tube radiant floor systems, (ii) validating experimentally the three aforementioned TRNSYS types (which have been validated qualitatively only), and (iii) providing a mathematical explanation of Type 993 (whose description is still unavailable to TRNSYS users). A sensitivity analysis is also performed to estimate the impact of the different types' parameters.

Keywords: *embedded-tube radiant floor systems; TRNSYS models; experimental measurements; sensitivity analysis*

1. INTRODUCTION

Embedded-tube radiant floors have been used in several buildings applications such as heating or cooling rooms (Rey and Zmeureanu, 2018) as well as in infrastructure applications such as de-icing of bridges and roads (Mauro and Grossman, 2017). Radiant floors can store and release significant amounts of thermal energy, which can improve thermal comfort (Olesen, 2002) and energy savings (Gwerder et al., 2008). As shown in (Hilliard et al., 2017), peak load reductions can be achieved through the use of model-based predictive control (MPC). MPC encompasses control methods which require a dynamic model of a process to minimize the difference between predicted and desired outputs. The performance of a MPC strategy therefore depends on reliable predictions from its underlying dynamic model. As mentioned in (Privara et al., 2013), building models account for the most time-consuming part in the design of MPC strategies. Building models should therefore combine flexibility with an appropriate level of complexity (Athienitis and O`Brien, 2015). Building performance simulation (BPS) tools provide different ways of modelling embedded-tube radiant floors. An inter-model comparison of radiant floor models from three different BPS tools, including TRNSYS (Klein et al., 2018), was conducted in (Brideau et al., 2015). TRNSYS is one of the most widely used BPS software, due to its capability to solve complex problems by coupling subroutines that model subsystem components (Beckman et al., 1994). Three different TRNSYS components (Type 56, Type 653, and Type 993) are available to model embedded-tube radiant floors. This paper aims at: (i) evaluating the appropriate model resolution for embedded-tube radiant floors, (ii) validating experimentally the three aforementioned TRNSYS types (which have been validated qualitatively only), and (iii) providing a mathematical explanation of Type 993 (whose description is still unavailable to TRNSYS users). A sensitivity analysis is conducted to assess the impact of the different types' parameters.

2. EMBEDDED-TUBE RADIANT FLOOR DESCRIPTION

An embedded-tube radiant floor experimental set-up was installed in a perimeter zone test hut (PTH) built inside an environmental chamber at Concordia University, as shown in **Figure 1**.

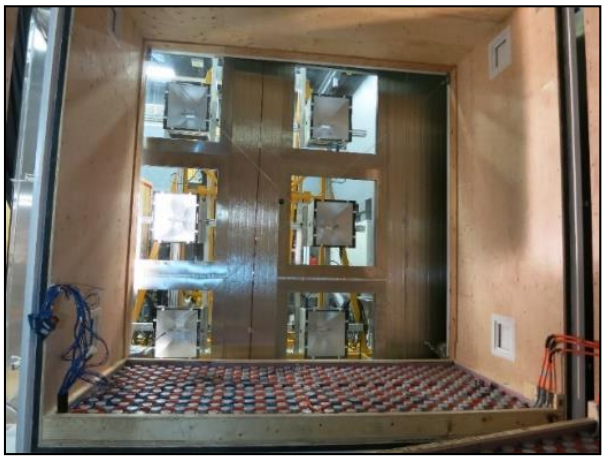

Figure 1: Perimeter zone test hut (PTH)

The floor of the PTH is composed of two nearly identical sections, referred to as the front (near the façade of the room) and back sections. As depicted in **Figure 2**, both sections contain an embedded-tube radiant floor, whose tubes are made of cross-linked polyethylene with an internal diameter of 1/2'' (12.7 mm) and wall thickness of 1/16'' (15.9 mm).

Figure 2: Front and back sections of the embedded-tube radiant floor set-up

A separation of 150 mm between the tubes is ensured by a rigid insulation foam matrix (see **Figure 3**) on top of which 80 mm of concrete was poured. The whole embedded-tube radiant floor (concrete layer and R-10 insulation foam matrix) is enclosed within a wooden frame.

Figure 3: Cylindrical insulation foam matrix

A 50% ethylene-glycol water mixture is used as a heat-transfer fluid within the tubing system with an average flow rate of approximately 0.4 gpm (90.8 kg/h) for the front section and 0.5 gpm (113.6 kg/h) for the back section. Without loss of generality, the rest of this paper focuses on the front section of the embedded-tube radiant floor experimental set-up, whose key characteristics can be found in **Table 1**.

Table 1: Main characteristics of the front section of the embedded-tube radiant floor experimental set-up

Characteristic	**Value**	**Unit**
Radiant floor experimental set-up		
Length	3150	mm
Width of the front section	1450	mm
Thickness	800	mm
Concrete properties		
Thermal conductivity	1.7	W/(m·°C)
Specific heat capacity	800	J/(kg·°C)
Volumetric density	2010	kg/m^3
Tubing properties		
Length of the front section	33850	mm
Internal diameter	12.7	mm
External diameter	15.9	mm
Thermal conductivity	0.41	W/(m·°C)
Fluid properties		
Specific heat capacity	3300	J/(kg·°C)
Insulation properties		
Thermal resistance	1.76	$(m^2 \cdot °C)/W$

3. TRNSYS MODELING

This section presents the three different models of the embedded-tube radiant floor experimental set-up and different assumptions which have been made in TRNSYS 18.

3.1 Type 56: Multi-Zone Building

Type 56 corresponds to a multi-zone building; however, users can insert an *active layer* to model an embedded-tube radiant floor (where the supply fluid temperature is an input of the multi-zone building model). The heat transfer from the tube to the core of the slab is calculated using a resistance approach, which is then linked to the TRNSYS transfer function formulation to describe the heat flow from the core slab to its top and bottom. A detailed mathematical

description of the embedded-tube radiant floor system is provided in the TRNSYS documentation. As mentioned in (Brideau et al., 2015), Type 56 is limited to certain radiant floor system configurations due to minimum thickness criteria depending on the spacing between the tubes. For this experimental set-up, the TRNSYS active layer is sandwiched in between two layers, whose top layer has a thickness of 73 mm (equivalent concrete thickness removing the cylindrical insulation foam matrix). The convective heat transfer coefficient for the embedded-tube radiant floor system can be either defined by users or internally calculated. The former was used as the latter yielded higher discrepancies between the measurements and predictions.

3.2 Type 653: Simple floor heating system

Type 653 is based on two main assumptions: (i) the slab of the embedded-tube radiant floor can be treated as a lumped capacitance, and (ii) the energy transfer from the fluid within the piping to the slab can be modeled using the heat exchanger effectiveness approach. A system whose internal temperature difference is small during a heat transfer process can be approximated by a lumped capacitance, which is spatially uniform in temperature. The lumped capacitance approximation implies that temperature gradients within the system are negligible, which means that the system's internal temperature depends on time only, that is, $T = T(t)$.

The heat exchanger (HX) effectiveness approach (or effectiveness-NTU approach) uses the heat transfer effectiveness ε of a heat exchanger, which is a dimensionless parameter, to find its heat transfer rate as follows:

$$\varepsilon = \frac{\dot{Q}}{\dot{Q}_{max}} \tag{1}$$

where $\dot{Q}$ and $\dot{Q}_{max}$ are the heat transfer and maximum possible heat transfer rates [kW], respectively. The maximum possible heat transfer rate depends on the maximum temperature difference between the two media involved ΔT_{max}, which is expressed as follows:

$$\Delta T_{max} = T_{h,in} - T_{c,in} \tag{2}$$

where $T_{h,in}$ and $T_{c,in}$ are the temperatures of the hot and cold media [°C], respectively.

The maximum possible heat transfer rate between the two media occurs when: (i) the cold medium is heated to the hot medium temperature, or (ii) the hot medium is cooled to the cold one. Since the thermal energy given by one medium must be absorbed by the other, the medium which undergoes the maximum temperature change would be the one with the minimum capacitance C_{min}. As a result, the maximum possible heat transfer rate is therefore calculated as follows:

$$\dot{Q}_{max} = C_{min} \cdot \left(T_{h,in} - T_{c,in}\right) = \min\left(\left(\dot{m}_h \cdot c_{p,h}\right), \left(\dot{m}_c \cdot c_{p,c}\right)\right) \cdot \left(T_{h,in} - T_{c,in}\right) \tag{3}$$

where $\dot{m}_h$ and $\dot{m}_c$ are the mass flow rates of the hot and cold media [kg/s], respectively; and $c_{p,h}$ and $c_{p,c}$ are the specific heat capacities at constant pressure of the hot and cold media [kJ/(kg·°C)], respectively.

The heat exchanger effectiveness approach reduces significantly the complex piping configuration dependent heat transfer between the two media, which are the fluid within the embedded tubes and the slab. Nevertheless, this parameter is difficult to estimate with certainty.

3.3 Type 993: Detailed radiant floor

Type 993 is a detailed model that performs a three-dimensional energy balance of the embedded-tube radiant floor system. The total number of pipes must be specified. Each pipe section is regarded as a separate pipe, whose inlet and direction are determined by the user. When the i-th pipe receives heat-transfer fluid from the (i-1)-th pipe, the inlet number of the i-th pipe is (i-1). The direction of the pipe is either towards the positive y-axis (direction number equal to 1) or towards the negative y-axis (direction number equal to 2). The inlet of one pipe section can therefore be defined as the outlet of another pipe section in order to construct the embedded-tube radiant floor system. A three-dimensional energy balance is then performed for each node, which yields a differential equation in the form:

$$\frac{dT}{dt} = aT + b \tag{4}$$

in which a and b are coefficients defined by the energy balances. For instance, the fluid temperature involves:

$$a = -\frac{\dot{m}_f}{m_f} - \frac{UA_{rad}}{m_f c_{p,f}} \tag{5}$$

$$b = \frac{\dot{m}_f T_{in,f}}{m_f} + \frac{UA_{radial} T_{slab,avg}}{m_f c_{p,f}} \quad (6)$$

where $\dot{m}_f$ is the heat-transfer fluid mass flow rate [kg/h]; m_f is the heat-transfer fluid mass contained in a given fluid node [kg]; UA_{radial} is the overall heat transfer coefficient to the adjacent soil nodes from the heat-transfer fluid [W/(m^2 · °C)]; $c_{p,f}$ is the specific heat capacity at constant pressure of the heat-transfer fluid [J/(kg·°C)]; $T_{in,f}$ and $T_{slab,avg}$ are the heat-transfer fluid temperature entering the fluid node and the average slab temperature around the pipe section [°C], respectively.

The fluid temperature can then be found by analytically solving **Equation (4)**. A three-dimensional energy balance is also applied to each slab node, which yields a differential equation in the form of **Equation (4)**, where the coefficients a and b are defined by the associated energy balance (which takes into account the heat transfer at each surface of the slab node as well as that at the pipe surface). The slab temperature can then be found by analytically solving the same type of differential equation. Due to its three-dimensional approach, Type 993 is extremely computationally expensive (180 times slower than Type 56 and Type 653, that is, 15 min when running on Windows 7 with an Intel Core i5-6200U@2.40 Hz having 8.0 GB RAM).

All these aforementioned types require input factors (inputs that are not directly related to the experimental measurements) or parameters, some reported in **Table 2**, which cannot be known without some degree of uncertainty.

Table 2: List of the main input factors and parameters of each TRNSYS type

Characteristic	**Parameter**	**Type**	**Nominal value**	**Unit**
Input factors				
Convective heat-transfer coefficient	1	56 / 653 / 993	2.7 (cooling) / 10.5 (heating)	W/(m^2·°C)
Top radiative loss temperature	2	653 / 993	From Type 56	°C
HX effectiveness	3	653	0.28	-
Parameters				
Length of the slab	4	56* / 653 / 993	3150	mm
Width of the slab	5	56* / 653 / 993	1450	mm
Thickness of the slab	6	56* / 653 / 993	73	mm
Slab/concrete thermal conductivity	7	56 / 993	1.7	W/(m·°C)
Slab volumetric density	8	56 / 653 / 993	2010	kg/m^3
Slab specific heat capacity	9	56 / 653 / 993	800	J/(kg·°C)
Bottom slab thermal resistance	10	56 / 653 / 993	1.76	(m^2·°C)/W
Top slab emissivity	11	56 / 653 / 993	0.95	-
Total pipe length	12	653 / 993*	33850	mm
Pipe inside diameter	13	56* / 653 / 993	12.7	mm
Pipe outside diameter	14	56 / 653 / 993	14.3	mm
Pipe wall conductivity	16	56 / 993	0.41	W/(m·°C)
Pipe spacing (center to center)	17	56 / 993*	150	mm
Fluid specific heat capacity	18	56 / 653 / 993	3300	J/(kg·°C)
Fluid volumetric density	19	653 / 993	1055	kg/m^3

* The same information can be required indirectly. For instance, the pipe inside diameter is not required for Type 56, but the outside diameter and thickness of the pipe are.

4. TRNSYS MODEL COMPARISON

This section presents a set-response experiment, which was conducted inside the environmental chamber at Concordia University, and a comparison between the three TRNSYS types.

4.1 Set-response experiment

A step-response experiment was conducted in the environmental chamber as follows:

1. The ambient air temperature of the PTH was set at approximately -4°C for a 24-h period in order for the PTH and embedded-tube radiant floor system to reach steady-state conditions;

2. The embedded-tube radiant floor system was activated at 10:30 on February 23, then deactivated at 12:58 on February 24, 2017. As shown in **Figure 4**, the heat-transfer fluid, whose supply temperature was fluctuating between 30°C and 35°C due to an on/off controller with dead-band, circulated over this 26-h period with a volumetric flow rate of approximately 0.4 gpm (90.8 kg/h) and 0.5 gpm (113.6 kg/h) in the front and back sections, respectively. The PTH's ambient air temperature was maintained at -4°C during the entire set-response experiment.

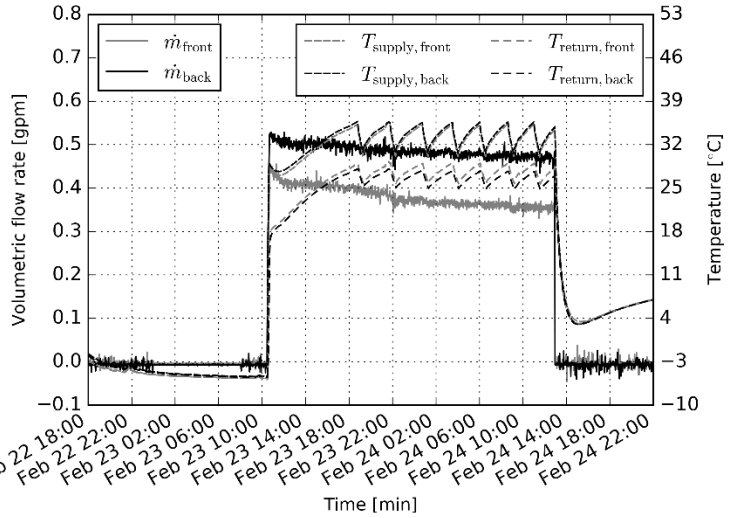

Figure 4: Volumetric flow rates as well as supply and return temperatures of the heat-transfer fluid into both sections of the radiant floor system

Seven thermocouples were distributed over the surface of each section of the embedded-tube radiant floor system to calculate the surface average temperature, as depicted in **Figure 5**. The measurements showed that the slab surface temperature was relatively uniform after reaching steady-state conditions (eight hours after activating the system).

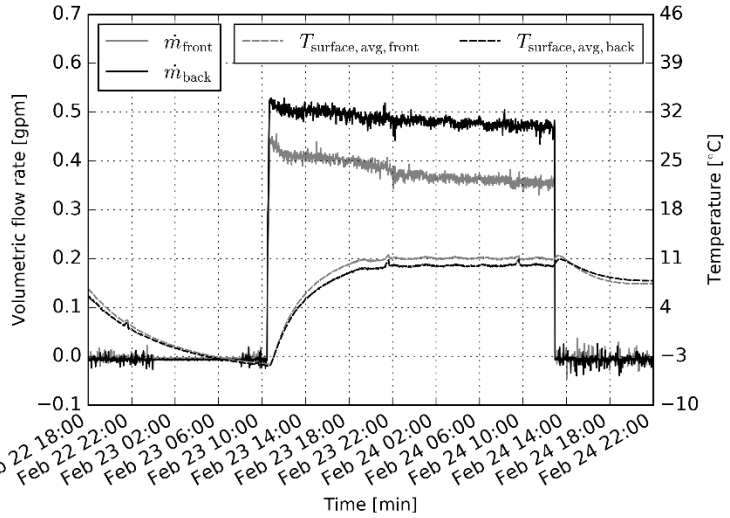

Figure 5: Volumetric flow rates of the heat-transfer fluid into and surface average temperatures of both sections of the radiant floor system

Given the volumetric flow rate and supply temperature, the three TRNSYS models are used to estimate the return and surface average temperatures. The top surface heat transfer rate could also be used to compare the TRNSYS models; however, temperatures are considered to be more easily understandable.

4.2 Simulation results

Figures 6 to 7 show the return and surface average temperatures measured and simulated using Type 56, Type 653, and Type 993, respectively. A time step of 1 min is used for the TRNSYS simulations (in accordance with the measurements)

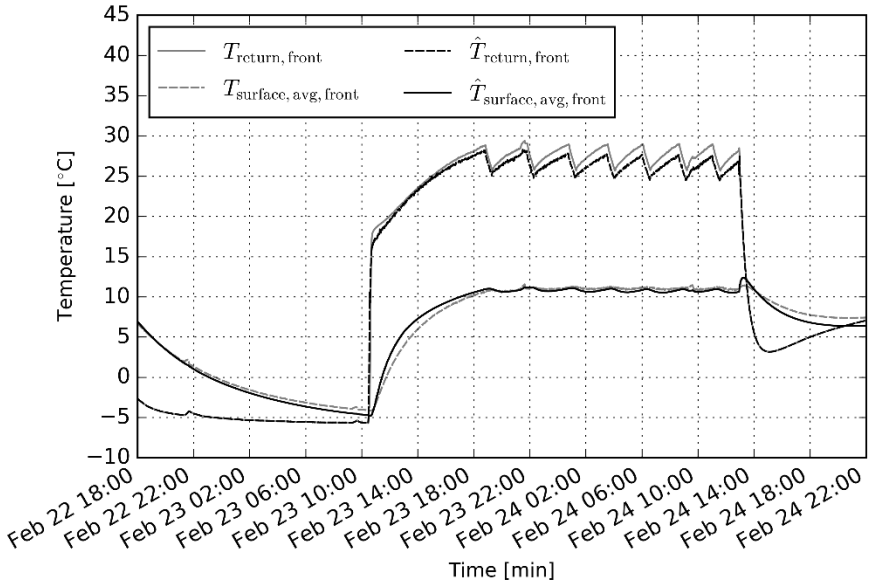

Figure 6: Return and surface average temperatures of the heat-transfer fluid within the front section of the radiant floor system measured and simulated using Type 56

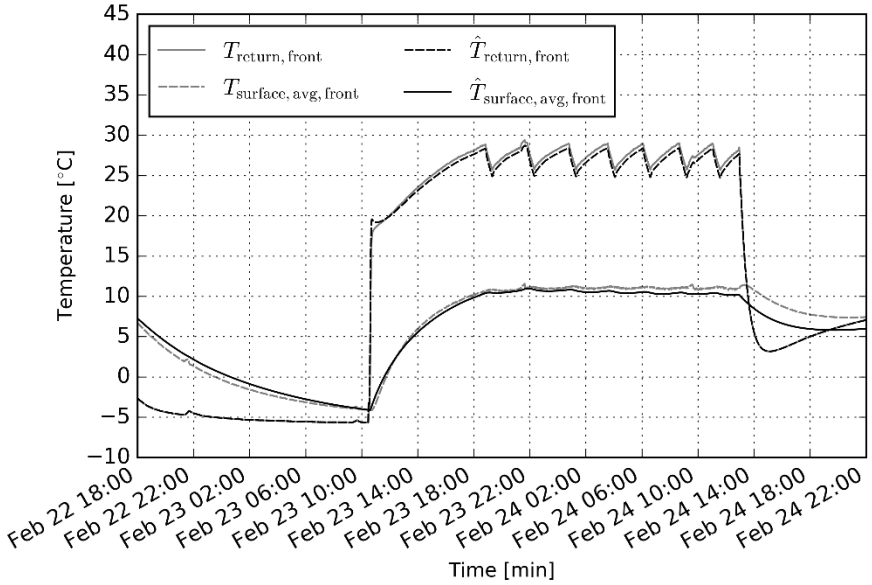

Figure 7: Return and surface average temperatures of the heat-transfer fluid within the front section of the radiant floor system measured and simulated using Type 653

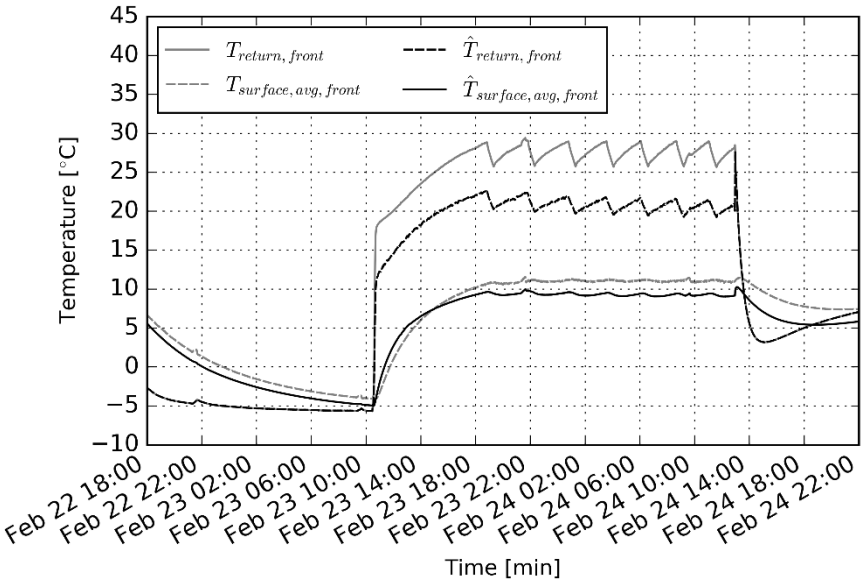

Figure 8: Return and surface average temperatures of the heat-transfer fluid within the front section of the radiant floor system measured and simulated using Type 993

As data visualization can be misleading, statistical indices are used to quantify how well the TRNSYS models describe the variability in the measurements. Two metrics are used to validate the TRNSYS models: (i) normalized mean bias error (NMBE) and (ii) coefficient of variation of the root mean squared error (CVRMSE). The NMBE is defined as (ASHRAE, 2002; Reddy, 2011):

$$\text{NMBE} = 100 \times \frac{\sum_{i=1}^{n}(y_i - \hat{y}_i)}{(n-p)\bar{y}} \tag{7}$$

where y_i is the i-th variable observation; $\hat{y}_i$ is the i-th simulation-predicted value of the observed variable; n is the number of variable observations; p is the number of parameters, set equal to 1 (ASHRAE, 2002); $\bar{y}$ is the arithmetic mean of the variable observations.

The CVRMSE is a normalized measure of dispersion, which is computed as follows (ASHRAE, 2002; Reddy, 2011):

$$\text{CVRMSE} = 100 \times \frac{\text{RMSE}}{\bar{y}} \tag{8}$$

in which RMSE is the root-mean-square error calculated as (ASHRAE, 2002; Reddy, 2011):

$$\text{RMSE} = \sqrt{\frac{\sum_{i=1}^{n}(y_i - \hat{y}_i)^2}{(n-p)}} \tag{9}$$

Table 3 reports the NMBE and CVRMSE values of the return and surface average temperatures for each TRNSYS type.

Table 3: Statistical indices of the difference between measured and predicted return and surface average temperatures

Statistical index	**Type 56**		**Type 653**		**Type 993**	
	T_{return} [°C]	$T_{surf,avg}$[°C]	T_{return} [°C]	$T_{surf,avg}$[°C]	T_{return} [°C]	$T_{surf,avg}$[°C]
NMBE [%]	2.21	0.75	0.03	4.14	24.03	11.60
CVRMSE [%]	5.91	3.31	1.70	6.38	37.18	11.28

The simulated temperatures fit well the measurements, as supported by **Figures 6 to 7** and **Table 3**; however, as mentioned in **Section 3**, each TRNSYS type depends on several parameters which cannot be known without any uncertainty. The value of some of these parameters was selected based on the experimental measurements through a simple calibration process by trial and error. A sensitivity analysis is therefore conducted to assess the impact of the different types' parameters as predictions cannot always rely on calibration.

4.3 Sensitivity analysis

As these TRNSYS types require several parameters, a sensitivity analysis is used to find a reduced list of key parameters, which could help future modeler choose only some relevant parameters leaving the others as default. The local effect of each parameter is found by computing the output partial derivative with respect to each parameter. The discretized approach proposed in (Morris, 1991) is used as follows:

$$\mathrm{S}_i = x_i \frac{\partial \hat{y}}{\partial x_i} = x_i \frac{\Delta \hat{y}}{\Delta x_i} = x_i \frac{[\hat{y}(x_1, x_2, \cdots, x_i + \Delta x_i, \cdots, x_k) - \hat{y}(x_1, x_2, \cdots, x_i, \cdots, x_k)]}{\Delta x_i} \quad (10)$$

where x_i is the i-th parameter's nominal value; Δx_i is the parameter increment, a multiple $1/(p-1)$ in which p is the level number.

An overview of the relative impact of each parameter can be obtained by normalizing the sensitivity index as follows:

$$\underline{\mathrm{S}}_i = \frac{S_i}{S_{max}} \quad (11)$$

where S_{max} is the maximum sensitivity index among all the parameters.

Some Type 653 parameters are increased by 5% around the nominal values (reported in **Table 2**). When the normalized sensitivity index is positive, the variation increases the output value. When it is negative, the variation decreases the output value. The output value chosen for the sensitivity analysis is the CVRMSE of both the return and surface average temperatures.

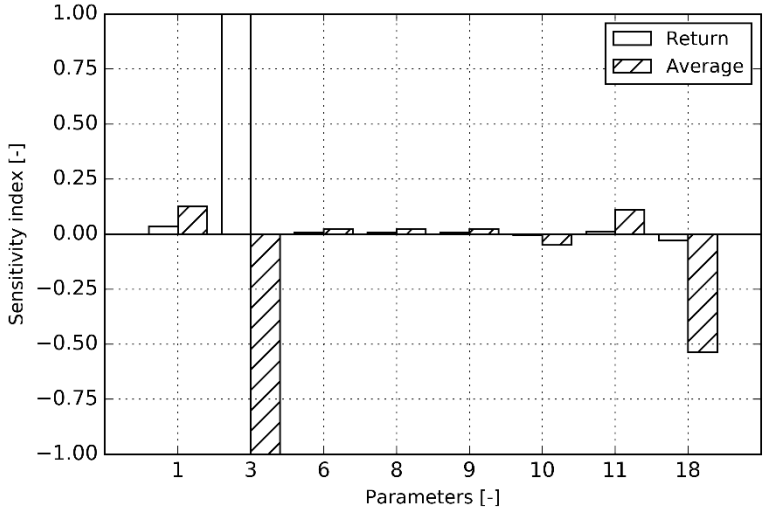

Figure 9: Sensitivity analysis of Type 653 parameters using the CVRMSE of the return and surface average temperatures

As show in **Figure 9**, the HX effectiveness has the highest impact on the predicted return and surface average temperatures followed by the heat transfer-fluid heat capacity. Increasing the nominal value of the heat transfer-fluid heat capacity by 5% improves both predicted temperatures.

4. CONCLUSIONS

Three different TRNSYS types (Type 56, Type 653, and Type 993) were presented, and then used to model an embedded-tube radiant floor experimental set-up. Due to its default configuration (i.e., tube in the middle of the slab), Type 993 showed discrepancies compared to Type 56 and 653, which were able to predict well the behavior of the

radiant floor system after a simple calibration process by trial and error; however, predictions cannot always rely on calibration. Several parameters are required for each type (the more detailed the type is, the more parameters are needed), which can lead to discrepancies between predictions and experimental measurements when such parameters are not well-known. Type 653 requires the HX effectiveness of the radiant floor system (which is difficult to determine without any data). Type 993 is extremely computationally expensive and require more parameters. As a result, Type 56 appears to be more appropriate outside of its own limitations (thin slab configuration), which highlights the importance of an appropriate level of complexity. Future work could include a more thorough sensitivity analysis.

NOMENCLATURE

Abbreviation		
BPS	Building Performance Simulation	(-)
CVRMSE	Coefficient of variation of the root mean squared error	(-)
HX	Heat Exchanger	(-)
MPC	Model-based Predictive Control	(-)
NMBE	Normalized Mean Bias Error	(-)
PTH	Perimeter zone Test Hut	(-)
RMSE	Root-Mean-Square Error	(-)

REFERENCES

ASHRAE (2002). *Guideline 14-2002: Measurement of Energy and Demand Savings*, Atlanta, Georgia, USA: American Society of Heating, Ventilating, and Air Conditioning Engineers.

Athienitis, A., and O`Brien, W. (2015). Modeling, design, and optimization of net-zero energy buildings. John Wiley & Son.

Broman, L., Fiksel, A., Klein, S. A., and Lindberg, E. (1994). TRNSYS, the most complete solar energy system modeling and simulation software. *Renewable Energy, 5*(1-4), 486-488.

Beckman, W. A., Broman, L., Fiksel, A., Klein, S. A., and Lindberg, E. (1994). TRNSYS, the most complete solar energy system modeling and simulation software. *Renewable Energy, 5*(1-4), 486-488.

Brideau, S. A., Beausoleil-Morrison, I., Kummert, M., and Wills, A. (2016). Inter-model comparison of embedded-tube radiant floor models in BPS tools. *Journal of Building Performance Simulation, 9*(2), 190-209.

Gwerder, M., Lehmann, B., Tödtli, J., Dorer, V., and Renggli, F. (2008). Control of thermally-activated building systems (TABS). *Applied energy, 85*(7), 565-581.

Hillard, T., Swan, L., and Qin, Z. (2017). Experimental implementation of whole building MPC with zone based thermal comfort adjustments. *Building and Environment, 125*, 326-338.

Klein, S. A., Du_e, J. A., Mitchell, J. C., Kummer, J. P., Thornton, J. W., Bradley, D. E., ..., and Kummert, M. (2018). *TRNSYS 18: A Transient System Simulation Program*. Solar Energy Laboratory, University of Wisconsin, Madison, USA. Retrieved on February 23, 2018, from http://sel.me.wisc.edu/trnsys/index.html

Mauro, A., and Grossman, J. C. (2017). Street-heat: Controlling road temperature via low enthalpy geothermal energy. *Applied Thermal Engineering, 110*, 1653-1658.

Morris, M. D. (1991). Factorial Sampling Plans for Preliminary Computational Experiments. *Technometrics, 33*(2), 161-174.

Olesen, B. W. (2002). Radiant floor heating in theory and practice. *ASHRAE journal, 44(*7), 19-24.

Privara, S., Cigler, J., Váňa, Z., Oldewurtel, F., Sagerschnig, C., and Žáčeková, E. (2013). Building modeling as a crucial part for building predictive control. *Energy and Buildings, 56*, 8-22.

Reddy T.A. (2011). *Applied Data Analysis and Modeling for Energy Engineers and Scientists*, New York, USA: Springer.

Rey, A., and Zmeureanu, R. (2018). Multi-objective optimization framework for the selection of configuration and equipment sizing of solar thermal combisystems. *Energy, 145*, 182-194.

ACKNOWLEDGEMENT

The authors would like to acknowledge the financial support received from Natural Sciences and Engineering Research Council of Canada, and from Faculty of Engineering and Computer Science of Concordia University as well as M. Saberi Derakhtenjani for providing us with experimental measurements.